PERGAMON

International Journal of Solids and Structures 39 (2002) 2129–2151

INTERNATIONAL JOURNAL OF SOLIDS and STRUCTURES

www.elsevier.com/locate/ijsolstr

Analytical solution for free vibration of piezoelectric coupled moderately thick circular plates

X. Liu, Q. Wang *, S.T. Quek

Department of Civil Engineering, National University of Singapore, 1 Engineering Drive 2, Singapore 117576, Singapore

Received 23 July 2001; received in revised form 11 December 2001

Abstract

An analytical model for free vibration analysis of piezoelectric coupled moderately thick circular plate is presented based on Mindlin's plate theory for the cases where electrodes on the piezoelectric layers are shortly connected. The distribution of electric potential along the thickness direction is simulated by a sinusoidal function. The differential equations of motion are solved analytically for two boundary conditions of the plate: clamped edge and simply supported edge. The detailed mathematical derivations are presented. Numerical investigations are performed for plates with two surface-bonded piezoelectric layers for various diameter–thickness ratios and the results are verified by those obtained from three-dimensional finite element analyses (ABAQUS 6.1). © 2002 Published by Elsevier Science Ltd.

Keywords: Piezoelectric; Plate; Analytical; Mindlin; Electric potential

1. Introduction

Since piezoelectric material has been widely used as actuators and sensors in smart structures, a study on modelling of a piezoelectric coupled structure is necessary and has been addressed by a lot of researchers. Beams with surface-bonded or embedded piezoelectric sensors and actuators were first analysed (Bailey and Hubbard, 1985; Crawley and de Luis, 1987). Different from the model based on a Euler beam assumption proposed by Crawley and Anderson (1989), Aldraihem and Khdeir (2000) used two shear deformation theories, the first-order beam theory (Timoshenko et al., 1974) and higher-order beam theory (Khdeir and Reddy, 1997, 1999), to model smart beams with shear- and extension-mode piezoelectric actuators.

Piezoelectric coupled plate modelling and analysis were also keenly researched. A three-dimensional solution of a plate is usually considered as an exact solution and used to verify the accuracy of the results provided by approximate theories, such as a two-dimensional plate theory. Bisegna and Maceri (1996) presented an exact three-dimensional solution for a simply supported transversely isotropic rectangular homogeneous piezoelectric plate. Heyliger (1997) obtained exact solutions for the static behaviour of laminated piezoelectric plates with simply support boundary condition. So and Leissa (1998) applied Ritz

* Corresponding author.
E-mail address: cvewangq@nus.edu.sg (Q. Wang).

0020-7683/02/$ - see front matter © 2002 Published by Elsevier Science Ltd.
PII: S0020-7683(02)00081-1

method in a three-dimensional analysis to obtain accurate frequencies for thick circular and annular plates with completely free edges, using trigonometric functions in the circumferential co-ordinate and algebraic polynomials in the radial and axial co-ordinates as the admissible functions. Even though three-dimensional models represent the plate behaviour more exactly than approximate methods, such as two-dimensional plate theories, they can only be solved analytically for some limited boundary conditions.

Due to their simplicity, two-dimensional models are still the most commonly used plate models. Refining the classical plate theory (CPT) (Love, 1944), Fernandes and Pouget (2001) and Almajid et al. (2001) performed analyses for thin piezoelectric laminated composites. Huang and Wu (1996) proposed two kinds of modification to the first-order shear deformation theory (Whitney and Pagano, 1970) to predict the static behaviour of hybrid multi-layered piezoelectric plates. To investigate the free vibration of piezoelectric laminate circular plates, Heyliger and Ramirez (2000) combined approximations of one-dimensional finite elements in the thickness direction and analytic functions in the plane within the context of the Ritz method. Yu (1995) derived equations of piezoelectric plates accounting for large deflections on the basis of CPT (Love, 1944) and refined plate theory (Mindlin, 1984). As early as 1952, Mindlin (1952) gave an analytical solution for forced flexural vibration of piezoelectric crystal plates. But no piezoeffects will be obtained since a linear distribution of electric potential is assumed across the thickness of piezoelectric plate if this model is applied to free vibration with two shortly connected electrodes bonded to the surfaces of piezoelectric plate.

The finite element method was also applied to analyse piezoelectric coupled structures (Hwang and Park, 1993; Chandrashekhara and Agarwal, 1993; Kim et al., 1996; Lam et al., 1997; Sheikh et al., 2001). Wang et al. (2000) proposed a two-dimensional finite element model by modifying the electric potential expansion proposed by Mindlin (1955, 1972) to satisfy the constant electric potential distribution on the surface with electrode. Three-dimensional finite element method accounting for piezoelectric materials has been implemented by commercial finite element analysis (FEA) codes ABAQUS (HKS Inc., 1993) and ANSYS (Swanson Inc., 1993). The finite element method is a powerful tool but sometimes an analytical solution is still needed to get a deep and clear understand of the mechanics of structural vibration.

There is a special interest in the modelling for piezoelectric coupled circular and annular plates since piezoelectric material can be used as actuator in ultrasonic motor (Lebrun et al., 1997). Hagood and McFarland (1995) developed an analytical model for a circular plate with a piezoelectric actuator by assuming that the distribution of electric potential is uniform in the radial direction. In fact, many published works on the mechanics model for the analysis of the piezoelectric coupled beams and plates adopted the assumption that the distribution of electric potential in the longitudinal direction of the piezoelectric layer is uniform and that in its thickness direction is linear, which may violate the Maxwell static electricity equation (Wang and Quek, 2000). Wang et al. (2001) assumed a quadratic distribution of electric potential across the thickness, which was verified by a 3-D FEA, to obtain the analytical solution for free vibration analysis of a piezoelectric coupled circular plate. Their analytical solution is applicable to only thin plates based on CPT.

In this paper, an analytical model for the free vibration analysis of piezoelectric coupled moderately thick circular plate is proposed. The displacement assumption follows the improved plate theory (IPT) (Mindlin, 1951a, 1951b). A sinusoidal function is adopted to describe the distribution of electric potential along the thickness direction. It is noted that the sinusoidal function has a similar shape to the quadratic one, but can make the governing equations simpler. The Maxwell static electricity equation is taken as one of the governing equations. The differential equations of motion are solved for two boundary conditions: clamped edge and simply supported edge and detailed mathematical derivations are presented. Numerical investigations are performed for plates bonded by two piezoelectric layers of various diameter–thickness ratios and the results are verified by the results of three-dimensional finite element analyses using ABAQUS 6.1. The results obtained by the CPT-based model (Wang et al., 2001) are also presented for comparison.

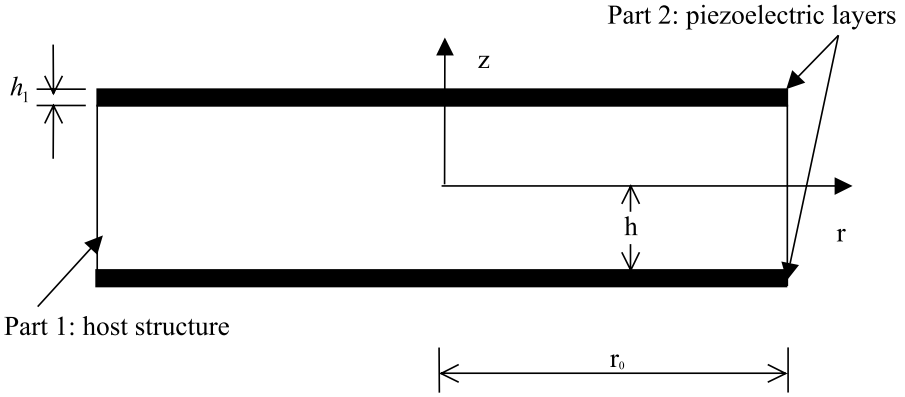

Fig. 1. Cross-section of a circular plate mounted with two piezoelectric layers.

2. Displacement and electric potential field models for circular plate

Fig. 1 shows the cross-section of a laminated circular plate comprising one host layer and two piezoelectric layers. Both top and bottom surfaces of each piezoelectric layer are fully covered by electrodes that are shortly connected. The plate has a radius of r_0 and the thickness of the host layer and each piezoelectric layer are $2h$ and h_1, respectively. The cylindrical coordinate system is adopted where the r–θ plane is coincident with the mid-plane of the undeformed plate.

2.1. Displacement field based on Mindlin's thick plate model

When thick plates are considered, the effect of shear deformation and rotary inertia cannot be omitted with negligible error. According to Mindlin (1951a,b) displacement fields of the plate are given by

$$u_z(r,\theta,z,t) = w(r,\theta,t), \tag{1}$$

$$u_r(r,\theta,z,t) = z\psi_r(r,\theta,t), \tag{2}$$

$$u_\theta(r,\theta,z,t) = z\psi_\theta(r,\theta,t), \tag{3}$$

where u_z, u_r, and u_θ are the displacements of the plate in the transverse, radial, and tangential direction, respectively; w is the transverse displacement of the mid-plane; and ψ_r and ψ_θ are the rotations of vertical lines perpendicular to the mid-plane, measured on the z–r and z–θ planes, respectively, as shown in Fig. 2. It is assumed that (a) there is no "thickness stretch" of the plate; (b) straight material lines that are perpendicular to the mid-plane in the undeformed state remain straight in the deformed state even though they may not remain perpendicular to the mid-plane.

The poling direction of the piezoelectric material is assumed to be in the z-direction. When external electric potential is applied across the piezoelectric layer, a differential strain is induced which results in the bending of the plate. The strain of the host plate and piezoelectric layer in the radial and tangential directions and the shear component are given by

$$\varepsilon_{rr} = \frac{\partial u_r}{\partial r} = z\frac{\partial \psi_r}{\partial r}, \tag{4}$$

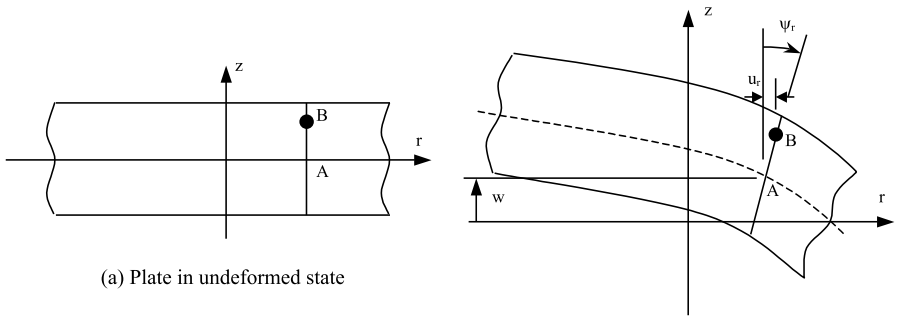

(a) Plate in undeformed state

(b) Plate in deformed state

Fig. 2. Deformation of plate.

$$\varepsilon_{\theta\theta} = \frac{u_r}{r} + \frac{\partial u_\theta}{r\partial\theta} = z\left(\frac{\psi_r}{r} + \frac{\partial\psi_\theta}{r\partial\theta}\right), \tag{5}$$

$$\gamma_{r\theta} = \frac{\partial u_r}{r\partial\theta} + \frac{\partial u_\theta}{\partial r} - \frac{u_\theta}{r} = z\left(\frac{\partial\psi_r}{r\partial\theta} - \frac{\psi_\theta}{r} + \frac{\partial\psi_\theta}{\partial r}\right), \tag{6}$$

$$\gamma_{rz} = \frac{\partial u_r}{\partial z} + \frac{\partial u_z}{\partial r} = \psi_r + \frac{\partial w}{\partial r}, \tag{7}$$

$$\gamma_{\theta z} = \frac{\partial u_\theta}{\partial z} + \frac{\partial u_z}{r\partial\theta} = \psi_\theta + \frac{\partial w}{r\partial\theta}. \tag{8}$$

The stress components in the host plate are expressed as

$$\sigma_{rr}^{(1)} = \frac{E}{1-\mu^2}(\varepsilon_{rr} + \mu\varepsilon_{\theta\theta}) = \frac{zE}{1-\mu^2}\left(\mu\frac{\psi_r}{r} + \mu\frac{\partial\psi_\theta}{r\partial\theta} + \frac{\partial\psi_r}{\partial r}\right), \tag{9}$$

$$\sigma_{\theta\theta}^{(1)} = \frac{E}{1-\mu^2}(\varepsilon_{\theta\theta} + \mu\varepsilon_{rr}) = \frac{zE}{1-\mu^2}\left(\frac{\psi_r}{r} + \frac{\partial\psi_\theta}{r\partial\theta} + \mu\frac{\partial\psi_r}{\partial r}\right), \tag{10}$$

$$\tau_{r\theta}^{(1)} = \frac{E}{2(1+\mu)}\gamma_{r\theta} = \frac{zE}{2(1+\mu)}\left(\frac{\partial\psi_\theta}{\partial r} - \frac{\psi_\theta}{r} + \frac{\partial\psi_r}{r\partial\theta}\right), \tag{11}$$

$$\tau_{rz}^{(1)} = \kappa^2\frac{E}{2(1+\mu)}\gamma_{rz} = \kappa^2\frac{E}{2(1+\mu)}\left(\psi_r + \frac{\partial w}{\partial r}\right), \tag{12}$$

$$\tau_{\theta z}^{(1)} = \kappa^2\frac{E}{2(1+\mu)}\gamma_{\theta z} = \kappa^2\frac{E}{2(1+\mu)}\left(\psi_\theta + \frac{\partial w}{r\partial\theta}\right), \tag{13}$$

where the superscript (1) represents the variable in the host structure; E and μ are the Young's modulus and Poisson ratio of the host material; and κ is the shear factor employed in Mindlin's plate model (Mindlin, 1951a, 1951b) to correct for the shear modulus, chosen as $\pi/\sqrt{12}$ here.

The stress components in piezoelectric layer can be written as

$$\sigma_{rr}^{(2)} = \overline{C}_{11}^{E}\varepsilon_{rr} + \overline{C}_{12}^{E}\varepsilon_{\theta\theta} - \bar{e}_{31}E_z, \tag{14}$$

$$\sigma_{\theta\theta}^{(2)} = \overline{C}_{12}^{E}\varepsilon_{rr} + \overline{C}_{11}^{E}\varepsilon_{\theta\theta} - \bar{e}_{31}E_z, \tag{15}$$

$$\tau_{r\theta}^{(2)} = \tfrac{1}{2}(\overline{C}_{11}^{E} - \overline{C}_{12}^{E})\gamma_{r\theta}, \tag{16}$$

$$\tau_{rz}^{(2)} = \kappa^2 C_{55}^{E}\gamma_{rz} + e_{15}E_r, \tag{17}$$

$$\tau_{\theta z}^{(2)} = \kappa^2 C_{55}^{E}\gamma_{\theta z} + e_{15}E_\theta, \tag{18}$$

where the superscript (2) represents the variable in the piezoelectric material; $\overline{C}_{11}^{E}$, $\overline{C}_{12}^{E}$ and $\bar{e}_{31}$ are the reduced material constants of the piezoelectric medium (see Appendix A), and are given by $\overline{C}_{11}^{E} = C_{11}^{E} - ((C_{13}^{E})^2/C_{33}^{E})$, $\overline{C}_{12}^{E} = C_{12}^{E} - ((C_{13}^{E})^2/C_{33}^{E})$ and $\bar{e}_{31} = e_{31} - (C_{13}^{E}e_{33}/C_{33}^{E})$; C_{11}^{E}, C_{33}^{E}, C_{12}^{E} and C_{55}^{E} are the moduli of elasticity at constant electric field; e_{31} and e_{15} are the piezoelectric electric constants; and E_r, E_θ and E_z are the electric field intensities in the radial, tangential and transverse direction, respectively.

2.2. Distribution of electric potential in the piezoelectric layer

For free vibration analysis with the electrodes on each piezoelectric layer short-circuited, a quadratic function was proposed and verified using FEA by Wang et al. (2001) to describe the electric potential distribution across the thickness of piezoelectric layers in piezoelectric coupled circular plates. In this paper a sinusoidal function is adopted instead so that a simpler governing equations can be obtained. The electric potential at any point of the piezoelectric layers is assumed as

$$\phi(r,\theta,z,t) = \begin{cases} \varphi(r,\theta,t)\sin\frac{\pi(z-h)}{h_1}, & h \leqslant z \leqslant h+h_1, \\ \varphi(r,\theta,t)\sin\frac{\pi(-z-h)}{h_1}, & -h-h_1 \leqslant z \leqslant -h, \end{cases} \tag{19}$$

where z is measured from the mid-plane of the plate in the transverse direction; h and h_1 are the thickness of the host layer and the piezoelectric layer, respectively; φ is the electric potential on the mid-surface of the piezoelectric layer. It is to be noted that the assumed potential function satisfies the boundary conditions that electric potential vanishes at the internal surfaces $z = \pm h$ and the external surfaces $z = \pm(h + h_1)$. The sinusoidal function employed here has a similar shape to that of the quadratic function adopted by Wang et al. (2001).

3. Equations for free vibration analysis of piezoelectric coupled circular plate

Based on the assumption of electric potential distribution across the thickness direction shown in (19), the components of electric field intensity E and electric flux density D can be written as

$$E_r = -\frac{\partial\phi}{\partial r} = -\frac{\partial\varphi}{\partial r}\sin\frac{\pi(z-h)}{h_1}, \tag{20}$$

$$E_\theta = -\frac{\partial\phi}{r\partial\theta} = -\frac{\partial\varphi}{r\partial\theta}\sin\frac{\pi(z-h)}{h_1}, \tag{21}$$

$$E_z = -\frac{\partial\phi}{\partial z} = -\frac{\pi\varphi}{h_1}\cos\frac{\pi(z-h)}{h_1}, \tag{22}$$

$$D_r = e_{15}\gamma_{rz} + \overline{\Xi}_{11}E_r = e_{15}\left(\psi_r + \frac{\partial w}{\partial r}\right) - \overline{\Xi}_{11}\frac{\partial\varphi}{\partial r}\sin\frac{\pi(z-h)}{h_1}, \tag{23}$$

$$D_\theta = e_{15}\gamma_{\theta z} + \overline{\Xi}_{11}E_\theta = e_{15}\left(\psi_\theta + \frac{\partial w}{r\partial\theta}\right) - \overline{\Xi}_{11}\frac{\partial\varphi}{r\partial\theta}\sin\frac{\pi(z-h)}{h_1}, \tag{24}$$

$$D_z = \bar{e}_{31}(\varepsilon_{rr}+\varepsilon_{\theta\theta}) + \overline{\Xi}_{33}E_z = z\bar{e}_{31}\left(\frac{\partial\psi_r}{\partial r}+\frac{\psi_r}{r}+\frac{\partial\psi_\theta}{r\partial\theta}\right) - \overline{\Xi}_{33}\frac{\pi\varphi}{h_1}\cos\frac{\pi(z-h)}{h_1}, \tag{25}$$

where D_r, D_θ and D_z are the corresponding electric displacement (electric flux density) components; $\overline{\Xi}_{11}$ and $\overline{\Xi}_{33}$ are the reduced dielectric constant of the piezoelectric layer, and are given by $\overline{\Xi}_{11} = \Xi_{11}$, $\overline{\Xi}_{33} = \Xi_{33} + e_{33}^2/C_{33}^E$ (see Appendix A); and Ξ_{11} and Ξ_{33} are the dielectric constants of the piezoelectric layer.

The resultant moments caused by the stresses are expressed, in view of Eqs. (9)–(18), as

$$\begin{aligned} M_{rr} &= \int_{-h-h_1}^{h+h_1} z\sigma_{rr}\,\mathrm{d}z = \int_{-h}^{h} z\sigma_{rr}^{(1)}\,\mathrm{d}z + 2\int_{h}^{h+h_1} z\sigma_{rr}^{(2)}\,\mathrm{d}z \\ &= (D_1+D_2)\frac{\partial\psi_r}{\partial r} + \left(\mu D_1 + \frac{\overline{C}_{12}^E}{\overline{C}_{11}^E}D_2\right)\left(\frac{\psi_r}{r}+\frac{\partial\psi_\theta}{r\partial\theta}\right) - \frac{4h_1\bar{e}_{31}}{\pi}\varphi, \end{aligned} \tag{26}$$

$$\begin{aligned} M_{\theta\theta} &= \int_{-h-h_1}^{h+h_1} z\sigma_{\theta\theta}\,\mathrm{d}z = \int_{-h}^{h} z\sigma_{\theta\theta}^{(1)}\,\mathrm{d}z + 2\int_{h}^{h+h_1} z\sigma_{\theta\theta}^{(2)}\,\mathrm{d}z \\ &= \left(\mu D_1 + \frac{\overline{C}_{12}^E}{\overline{C}_{11}^E}D_2\right)\frac{\partial\psi_r}{\partial r} + (D_1+D_2)\left(\frac{\psi_r}{r}+\frac{\partial\psi_\theta}{r\partial\theta}\right) - \frac{4h_1\bar{e}_{31}}{\pi}\varphi, \end{aligned} \tag{27}$$

$$M_{r\theta} = \int_{-h-h_1}^{h+h_1} z\tau_{r\theta}\,\mathrm{d}z = \int_{-h}^{h} z\tau_{r\theta}^{(1)}\,\mathrm{d}z + 2\int_{h}^{h+h_1} z\tau_{r\theta}^{(2)}\,\mathrm{d}z = A_1\left(\frac{\partial\psi_r}{r\partial\theta}+\frac{\partial\psi_\theta}{\partial r}-\frac{\psi_\theta}{r}\right), \tag{28}$$

where D_1, D_2 and A_1 are constants related to plate stiffness and are given by

$$D_1 = \frac{2Eh^3}{3(1-\mu^2)}, \quad D_2 = \tfrac{2}{3}h_1(3h^2+3hh_1+h_1^2)\overline{C}_{11}^E \quad \text{and} \quad A_1 = \frac{1}{2}\left[(1-\mu)D_1 + \left(1-\frac{\overline{C}_{12}^E}{\overline{C}_{11}^E}\right)D_2\right].$$

The resultant shear forces are expressed as

$$Q_r = \int_{-h-h_1}^{h+h_1}\tau_{rz}\,\mathrm{d}z = \int_{-h}^{h}\tau_{rz}^{(1)}\,\mathrm{d}z + 2\int_{h}^{h+h_1}\tau_{rz}^{(2)}\,\mathrm{d}z = A_3\left(\frac{\partial w}{\partial r}+\psi_r\right) - \frac{4h_1e_{15}}{\pi}\frac{\partial\varphi}{\partial r}, \tag{29}$$

$$Q_\theta = \int_{-h-h_1}^{h+h_1}\tau_{\theta z}\,\mathrm{d}z = \int_{-h}^{h}\tau_{\theta z}^{(1)}\,\mathrm{d}z + 2\int_{h}^{h+h_1}\tau_{\theta z}^{(2)}\,\mathrm{d}z = A_3\left(\frac{\partial w}{r\partial\theta}+\psi_\theta\right) - \frac{4h_1e_{15}}{\pi}\frac{\partial\varphi}{r\partial\theta}, \tag{30}$$

where $A_3 = \kappa^2(Eh/(1+\mu)) + 2\kappa^2C_{55}^E h_1$.

It is to be noted that M_{rr}, $M_{r\theta}$, $M_{\theta\theta}$, Q_r and Q_θ must satisfy the following dynamic equilibrium equations

$$\frac{\partial Q_r}{\partial r}+\frac{\partial Q_\theta}{r\partial\theta}+\frac{Q_r}{r} - \left(\int_{-h}^{h}\rho_1\frac{\partial^2u_z}{\partial t^2}\,\mathrm{d}z + 2\int_{h}^{h+h_1}\rho_2\frac{\partial^2u_z}{\partial t^2}\,\mathrm{d}z\right) = 0, \tag{31}$$

$$\frac{\partial M_{rr}}{\partial r}+\frac{\partial M_{r\theta}}{r\partial\theta}+\frac{M_{rr}-M_{\theta\theta}}{r} - Q_r - \left(\int_{-h}^{h}\rho_1 z\frac{\partial^2u_r}{\partial t^2}\,\mathrm{d}z + 2\int_{h}^{h+h_1}\rho_2 z\frac{\partial^2u_r}{\partial t^2}\,\mathrm{d}z\right) = 0, \tag{32}$$

$$\frac{\partial M_{r\theta}}{\partial r}+\frac{\partial M_{\theta\theta}}{r\partial\theta}+\frac{2M_{r\theta}}{r} - Q_\theta - \left(\int_{-h}^{h}\rho_1 z\frac{\partial^2u_\theta}{\partial t^2}\,\mathrm{d}z + 2\int_{h}^{h+h_1}\rho_2 z\frac{\partial^2u_\theta}{\partial t^2}\,\mathrm{d}z\right) = 0, \tag{33}$$

where ρ_1 and ρ_2 are the material densities of the host material and piezoelectric layer, respectively.

The electric variables must also satisfy the Maxwell's equations which require that the divergence of the electric flux density vanishes at any point within the piezoelectric layers. In the two-dimensional analysis of plate, this condition can be satisfied approximately by enforcing that the integration of the divergence of the electric flux density across the thickness of the piezoelectric layers vanishes all over the plate, namely for any r and θ,

$$\int_h^{h+h_1}\left(\frac{\partial(rD_r)}{r\partial r}+\frac{\partial D_\theta}{r\partial\theta}+\frac{\partial D_z}{\partial z}\right)\mathrm{d}z=0. \tag{34}$$

Substituting Eqs. (26)–(30) into Eqs. (31)–(33) and Eqs. (23)–(25) into Eq. (34) yield the equations of motion,

$$A_3(\Delta w+\Psi)-A_6\Delta\varphi-A_7\frac{\partial^2 w}{\partial t^2}=0, \tag{35}$$

$$\begin{aligned}&A_1\Delta\psi_r+A_2\frac{\partial(r\Psi)}{r\partial r}-A_3\left(\psi_r+\frac{\partial w}{\partial r}\right)-(D_1+D_2)\left(\frac{\psi_r}{r^2}+\frac{\partial\psi_\theta}{r^2\partial\theta}\right)-A_2\frac{\partial\psi_r}{r\partial r}-A_1\frac{\partial\psi_\theta}{r^2\partial\theta}+A_5\frac{\partial\varphi}{\partial r}\\&\quad-A_4\frac{\partial^2\psi_r}{\partial t^2}=0,\end{aligned} \tag{36}$$

$$A_1\Delta\psi_\theta+A_2\frac{\partial\Psi}{r\partial\theta}-A_3\left(\psi_\theta+\frac{\partial w}{r\partial\theta}\right)+2A_1\left(\frac{\partial\psi_r}{r^2\partial\theta}-\frac{\psi_\theta}{2r^2}\right)+A_5\frac{\partial\varphi}{r\partial\theta}-A_4\frac{\partial^2\psi_\theta}{\partial t^2}=0, \tag{37}$$

$$-\frac{2h_1\overline{\Xi}_{11}}{\pi}\Delta\varphi+h_1e_{15}\Delta w+\frac{2\pi\overline{\Xi}_{33}}{h_1}\varphi+h_1(e_{15}+\bar{e}_{31})\Psi=0, \tag{38}$$

where Δ is the Laplace operator and in polar coordinate system is given by

$$\frac{\partial^2}{\partial r^2}+\frac{\partial}{r\partial r}+\frac{\partial^2}{r^2\partial\theta^2}$$

Ψ is a function of ψ_r and ψ_θ, given by

$$\Psi=\frac{\partial\psi_r}{\partial r}+\frac{\psi_r}{r}+\frac{\partial\psi_\theta}{r\partial\theta}; \tag{39}$$

$A_1, A_2, A_3, A_4, A_5, A_6$ and A_7 are constants governed by material properties and structural geometry, given in Appendix B.

4. Solutions for piezoelectric coupled circular plates

In the four differential equation (35)–(38) there are four independent variables, w, ψ_r, ψ_θ and φ that need to be solved. The solution procedure is described hereafter. Note that the variable Ψ is not independent but a function of ψ_r and ψ_θ (see Eq. (39)).

4.1. Solutions for transverse displacement w

Eliminating ψ_r, ψ_θ and φ from Eqs. (35)–(38) yields an uncoupled differential equation in terms of w only, namely,

$$P_1\Delta\Delta\Delta w + P_2\Delta\Delta w + P_3\Delta\Delta\left(\frac{\partial^2 w}{\partial t^2}\right) + P_4\Delta\left(\frac{\partial^4 w}{\partial t^4}\right) + P_5\Delta\left(\frac{\partial^2 w}{\partial t^2}\right) + P_6\frac{\partial^2 w}{\partial t^2} + P_7\frac{\partial^4 w}{\partial t^4} = 0, \tag{40}$$

where the coefficients, P_1, P_2, P_3, P_4, P_5, P_6 and P_7, are given in Appendix B. The solution of $w(r,\theta,t)$ for wave propagation in the θ-direction can be written as

$$w(r,\theta,t) = \hat{w}(r)e^{i(p\theta-\omega t)}, \tag{41}$$

where $\hat{w}(r)$ is the amplitude of the z-direction displacement and a function of radial distance only; ω is the natural frequency of the plate; and p is the wave number in the θ-direction. Substituting Eq. (41) into Eq. (40) and cancelling $e^{i(p\theta-\omega t)}$ term gives

$$P_1\overline{\Delta}\overline{\Delta}\overline{\Delta}\hat{w} + (P_2 - P_3\omega^2)\overline{\Delta}\overline{\Delta}\hat{w} + (P_4\omega^4 - P_5\omega^2)\overline{\Delta}\hat{w} + (P_7\omega^4 - P_6\omega^2)\hat{w} = 0, \tag{42}$$

where $\overline{\Delta}$ is a operator defined as

$$\overline{\Delta} = \frac{d^2}{dr^2} + \frac{d}{rdr} - \frac{p^2}{r^2}.$$

Transforming Eq. (42) into the form

$$(\overline{\Delta} - x_1)(\overline{\Delta} - x_2)(\overline{\Delta} - x_3)\hat{w} = 0, \tag{43}$$

where x_1, x_2 and x_3 are the three roots of the cubic equation,

$$P_1x^3 + (P_2 - P_3\omega^2)x^2 + (P_4\omega^4 - P_5\omega^2)x + P_7\omega^4 - P_6\omega^2 = 0. \tag{44}$$

The solution of Eq. (42) takes the form of

$$\hat{w} = \hat{w}_1 + \hat{w}_2 + \hat{w}_3 \tag{45}$$

provided $\hat{w}_1$, $\hat{w}_2$ and $\hat{w}_3$ are solutions of the following three Bessel's equations, respectively:

$$\begin{aligned}(\overline{\Delta} - x_1)\hat{w}_1 &= 0,\\ (\overline{\Delta} - x_2)\hat{w}_2 &= 0,\\ (\overline{\Delta} - x_3)\hat{w}_3 &= 0,\end{aligned} \tag{46}$$

The transformation $x = y + (P_3\omega^2 - P_2)/3P_1$ eliminates the second-order term of Eq. (44), resulting in

$$y^3 + by + c = 0, \tag{47}$$

where

$$b = \frac{P_4\omega^4 - P_5\omega^2}{P_1} - \frac{(P_2 - P_3\omega^2)^2}{3P_1^2}, c = \frac{\omega^2(P_7\omega^2 - P_6)}{P_1} + \frac{\omega^2(P_5 - P_4\omega^2)(P_2 - P_3\omega^2)}{3P_1^2} + \frac{2(P_2 - P_3\omega^2)^3}{27P_1^3}. \tag{48}$$

The discriminant of the cubic equation is given by

$$\delta = \left(\frac{c}{2}\right)^2 + \left(\frac{b}{3}\right)^3. \tag{49}$$

In practice, $\delta < 0$ is usually satisfied. Thus, according to Cardano's formula (Speigel, 1999), the characteristic equation (44) has three distinct real roots given by

$$
\begin{aligned}
x_1 &= 2S\cos\frac{\gamma}{3} + \frac{P_3\omega^2 - P_2}{3P_1},\\
x_2 &= 2S\cos\frac{\gamma+2\pi}{3} + \frac{P_3\omega^2 - P_2}{3P_1},\\
x_3 &= 2S\cos\frac{\gamma+4\pi}{3} + \frac{P_3\omega^2 - P_2}{3P_1},
\end{aligned}
\tag{50}
$$

where

$$
S = \frac{1}{3}\sqrt{\frac{P_2^2 + (3P_1P_5 - 2P_2P_3)\omega^2 + (P_3^2 - 3P_1P_4)\omega^4}{P_1^2}}, \quad \gamma = \arccos\left[-\frac{c}{2\sqrt{(-\frac{b}{3})^3}}\right].
$$

In view of non-singularity of $\hat{w}$ at $r = 0$, the solution of Eq. (42) can be expressed as

$$
\hat{w} = \sum_{n=1}^{3} C_n Z_{np}(\alpha_n r), \tag{51}
$$

where $\alpha_1 = \sqrt{|x_1|}$, $\alpha_2 = \sqrt{|x_2|}$ and $\alpha_3 = \sqrt{|x_3|}$, C_n are constants and

$$
Z_{np}(\alpha_n r) = \begin{cases} J_p(\alpha_n r), & x_n < 0 \\ I_p(\alpha_n r), & x_n > 0 \end{cases} \quad (n = 1, 2, 3) \tag{52}
$$

in which $J_p(\alpha_i r)$ is the Bessel function of first type and $I_p(\alpha_i r)$ is the modified Bessel function of first type. It should be noted that the second type Bessel functions become singular at $r = 0$ and have been omitted from the solution.

4.2. Solutions for rotations ψ_r and ψ_θ

If the rotations ψ_r and ψ_θ are expressed in terms of the potential functions $\Phi(r, \theta, t)$ and $H(r, \theta, t)$ which give rise to areal dilatation and rotation

$$
\begin{aligned}
\psi_r &= \frac{\partial \Phi}{\partial r} + \frac{\partial H}{r\partial\theta},\\
\psi_\theta &= \frac{\partial \Phi}{r\partial\theta} - \frac{\partial H}{\partial r},
\end{aligned}
\tag{53}
$$

Eqs. (36) and (37) become

$$
\frac{\partial}{\partial r}\left[(D_1 + D_2)\,\Delta\Phi - A_3\Phi - A_4\frac{\partial^2\Phi}{\partial t^2} - A_3 w + A_5\varphi\right] + \frac{\partial}{r\partial\theta}\left[A_1\,\Delta H - A_3 H - A_4\frac{\partial^2 H}{\partial t^2}\right] = 0, \tag{54}
$$

$$
\frac{\partial}{r\partial\theta}\left[(D_1 + D_2)\Delta\Phi - A_3\Phi - A_4\frac{\partial^2\Phi}{\partial t^2} - A_3 w + A_5\varphi\right] - \frac{\partial}{\partial r}\left[A_1\,\Delta H - A_3 H - A_4\frac{\partial^2 H}{\partial t^2}\right] = 0. \tag{55}
$$

If applying the operator $\partial/r\partial\theta$ to Eq. (54), $(1/r + (\partial/r\partial r))$ to Eq. (55), and subtracting, we obtain a decoupled equation in terms of H,

$$
\Delta\left(A_1\,\Delta H - A_3 H - A_4\frac{\partial^2 H}{\partial t^2}\right) = 0. \tag{56}
$$

Similarly, application of the operator $(1/r + (\partial/r\partial r))$ to Eq. (54), $\partial/r\partial\theta$ to Eq. (55), and adding the results yield another decoupled equation free of H,

$$\Delta\left[(D_1+D_2)\Delta\Phi - A_3\Phi - A_4\frac{\partial^2\Phi}{\partial t^2} - A_3 w + A_5\varphi\right] = 0. \tag{57}$$

It is assumed that Φ, H, and φ take the form

$$\begin{aligned}
\Phi(r,\theta,t) &= \widehat{\Phi}(r)\mathrm{e}^{\mathrm{i}(p\theta-\omega t)},\\
H(r,\theta,t) &= \widehat{H}(r)\mathrm{e}^{\mathrm{i}(p\theta-\omega t)},\\
\varphi(r,\theta,t) &= \hat{\varphi}(r)\mathrm{e}^{\mathrm{i}(p\theta-\omega t)},
\end{aligned} \tag{58}$$

where $\hat{\varphi}(r)$, $\widehat{H}(r)$, and $\widehat{\Phi}(r)$ are amplitudes of $\varphi(r,\theta,t)$, $H(r,\theta,t)$ and $\Phi(r,\theta,t)$, respectively. Substituting Eqs. (41) and (58) into Eqs. (35), (56), (57), and (38) reduces to

$$A_3\overline{\Delta}\widehat{\Phi} + A_3\overline{\Delta}\hat{w} + A_7\omega^2\hat{w} - A_6\overline{\Delta}\hat{\varphi} = 0, \tag{59}$$

$$A_1\overline{\Delta}\widehat{H} - (A_3 - A_4\omega^2)\widehat{H} = 0, \tag{60}$$

$$(D_1+D_2)\overline{\Delta}\widehat{\Phi} - (A_3 - A_4\omega^2)\widehat{\Phi} - A_3\hat{w} + A_5\hat{\varphi} = 0, \tag{61}$$

$$\overline{\Delta}\widehat{\Phi} + A_8\overline{\Delta}\hat{w} - A_9\overline{\Delta}\hat{\varphi} + A_{10}\hat{\varphi} = 0, \tag{62}$$

where the coefficients, A_8, A_9, and A_{10}, are given in Appendix B. Solving Eq. (60) for $\widehat{H}$ gives

$$\widehat{H}(r) = C_{6a}Z_{6p}(\beta_1 r) + C_{7a}Z_{7p}(\beta_1 r), \tag{63}$$

where C_{6a} and C_{7a} are arbitrary constants;

$$\beta_1 = \sqrt{|F_1|}, \quad F_1 = \frac{A_3 - A_4\omega^2}{A_1}; \tag{64}$$

$$\begin{aligned}
Z_{6p}(\beta_1 r) &= \begin{cases} J_p(\beta_1 r), & F_1 < 0,\\ I_p(\beta_1 r), & F_1 > 0,\end{cases}\\
Z_{7p}(\beta_1 r) &= \begin{cases} Y_p(\beta_1 r), & F_1 < 0,\\ K_p(\beta_1 r), & F_1 > 0;\end{cases}
\end{aligned} \tag{65}$$

J_p and Y_p are the Bessel functions of the first kind and the second kind, respectively; and I_p and K_p are the modified Bessel functions of the first kind and the second kind, respectively. To avoid singularity at $r = 0$, $C_{7a} = 0$. Thus, Eq. (63) is reduced to

$$\widehat{H}(r) = C_{6a}Z_{6p}(\beta_1 r). \tag{66}$$

Solving Eqs. (59), (61), and (62) for $\widehat{\Phi}$ yields

$$\begin{aligned}
\widehat{\Phi}(r) = \frac{G_2/A_{10}}{A_{10}A_3A_6G_1 - A_3A_5 + A_3A_6 - A_4A_6\omega^2}\Bigg\{ & \frac{G_1(A_9A_3 - A_6A_8)}{A_3 - A_4\omega^2}\overline{\Delta}\overline{\Delta}\hat{w} + \Bigg[\frac{A_5(A_9A_3 - A_6A_8)}{G_2}\\
& + \frac{G_1(A_7A_9\omega^2 - A_3A_{10}) - A_3}{A_3 - A_4\omega^2} - \frac{A_3A_5(A_8 - 1)}{(A_6 - A_3A_9)(A_3 - A_4\omega^2)}\Bigg]\overline{\Delta}\hat{w}\\
& + \left[\frac{A_5A_9A_7\omega^2 - A_6A_{10}A_3}{G_2} - \frac{A_{10}A_3^2 + (A_{10}D_1 + A_{10}D_2 - A_5)A_7\omega^2}{(A_6 - A_3A_9)(A_3 - A_4\omega^2)}\right]\hat{w}\Bigg\}
\end{aligned} \tag{67}$$

Substituting Eqs. (51), (58), (66) and (67) into Eq. (53) and replacing iC_{6a} by C_6 yields

$$\begin{aligned}\psi_r(r,\theta,t) &= \left\{ \frac{G_2/A_{10}}{A_{10}A_3A_6G_1 - A_3A_5 + A_3A_6 - A_4A_6\omega^2} \sum_{n=1}^{3} \left[\frac{G_1(A_9A_3 - A_6A_8)x_n^2 + (G_1A_7A_9\omega^2 - G_1A_3A_{10} - A_3)x_n}{A_3 - A_4\omega^2} \right.\right. \\ &\quad + \frac{A_5(A_9A_3 - A_6A_8)x_n + A_5A_9A_7\omega^2 - A_6A_{10}A_3}{G_2} \\ &\quad \left.\left. - \frac{A_3A_5(A_8-1)x_n + A_{10}A_3^2 + (A_{10}D_1 + A_{10}D_2 - A_5)A_7\omega^2}{(A_6 - A_3A_9)(A_3 - A_4\omega^2)} \right] C_n\alpha_n Z'_{np}(\alpha_n r) + \frac{C_6 p Z_{6p}(\beta_1 r)}{r} \right\} e^{i(p\theta-\omega t)}, \end{aligned} \tag{68}$$

$$\begin{aligned}\psi_\theta(r,\theta,t) &= \left\{ \frac{pG_2/A_{10}}{A_{10}A_3A_6G_1 - A_3A_5 + A_3A_6 - A_4A_6\omega^2} \sum_{n=1}^{3} \left[\frac{G_1(A_9A_3 - A_6A_8)x_n^2 + (G_1A_7A_9\omega^2 - G_1A_3A_{10} - A_3)x_n}{A_3 - A_4\omega^2} \right.\right. \\ &\quad + \frac{A_5(A_9A_3 - A_6A_8)x_n + A_5A_9A_7\omega^2 - A_6A_{10}A_3}{G_2} \\ &\quad \left.\left. - \frac{A_3A_5(A_8-1)x_n + A_{10}A_3^2 + (A_{10}D_1 + A_{10}D_2 - A_5)A_7\omega^2}{(A_6 - A_3A_9)(A_3 - A_4\omega^2)} \right] \frac{C_n Z_{np}(\alpha_n r)}{r} + C_6\beta_1 Z'_{6p}(\beta_1 r) \right\} e^{i(p\theta-\omega t)}, \end{aligned} \tag{69}$$

where the coefficients, G_1 and G_2, are given in Appendix B.

4.3. Solutions for electric potential φ

Solving Eq. (61) for $\hat{\varphi}(r)$ yields

$$\hat{\varphi}(r) = -\frac{D_1 + D_2}{A_5}\overline{\Delta}\widehat{\Phi}(r) + \frac{A_3 - A_4\omega^2}{A_5}\widehat{\Phi}(r) + \frac{A_3}{A_5}\hat{w}(r). \tag{70}$$

Substituting Eqs. (51), (67), and (70) into Eq. (58) results in

$$\begin{aligned}\varphi(r,\theta,t) &= \sum_{n=1}^{3} \left\{ \frac{G_2(A_3 - A_4\omega^2 - D_1x_n - D_2x_n)}{A_5A_{10}(A_{10}A_3A_6G_1 - A_3A_5 + A_3A_6 - A_4A_6\omega^2)} \left[\frac{G_1(A_9A_3 - A_6A_8)x_n^2 + (G_1A_7A_9\omega^2 - G_1A_3A_{10} - A_3)x_n}{A_3 - A_4\omega^2} \right.\right. \\ &\quad + \frac{A_5(A_9A_3 - A_6A_8)x_n + A_5A_9A_7\omega^2 - A_6A_{10}A_3}{G_2} \\ &\quad \left.\left. - \frac{A_3A_5(A_8-1)x_n + A_{10}A_3^2 + (A_{10}D_1 + A_{10}D_2 - A_5)A_7\omega^2}{(A_6 - A_3A_9)(A_3 - A_4\omega^2)} \right] + \frac{A_3}{A_5} \right\} C_n Z_{np}(\alpha_n r) e^{i(p\theta-\omega t)}. \end{aligned} \tag{71}$$

4.4. Determination of frequencies by boundary conditions

In the proceeding sections we obtained explicit expressions for transverse displacement $w(r,\theta,t)$, rotations $\psi_r(r,\theta,t)$ and $\psi_\theta(r,\theta,t)$, and electric potential $\varphi(r,\theta,t)$, which are all functions of the frequency ω. To determine the frequency, the boundary conditions must be employed. Two kinds of boundary conditions, clamped edge and simply supported edges, are addressed.

(a) Clamped edge

For clamped edge at $r = r_0$, both the transverse displacement w and rotations ψ_r and ψ_θ vanish, namely,

$$\begin{aligned} &w(r_0,\theta,t) = 0,\\ &\psi_r(r_0,\theta,t) = 0,\\ &\psi_\theta(r_0,\theta,t) = 0, \end{aligned} \tag{72}$$

where r_0 is radius of the plate. If the plate is isolated at the edge, the electrical flux conservation equation is given by

$$\int_h^{h+h_1} D_r(r_0,\theta,t)\,\mathrm{d}z = 0. \tag{73}$$

Substituting the solutions obtained in the proceeding sections for w, ψ_r, ψ_θ, and φ into Eqs. (72) and (73) and some simplifications yield

$$\begin{pmatrix} s_{11}^{(a)} & s_{12}^{(a)} & s_{13}^{(a)} & 0\\ s_{21}^{(a)} & s_{22}^{(a)} & s_{23}^{(a)} & s_{26}^{(a)}\\ s_{31}^{(a)} & s_{32}^{(a)} & s_{33}^{(a)} & s_{36}^{(a)}\\ s_{41}^{(a)} & s_{42}^{(a)} & s_{43}^{(a)} & 0 \end{pmatrix} \begin{pmatrix} C_1\\ C_2\\ C_3\\ C_6 \end{pmatrix} = \begin{pmatrix} 0\\ 0\\ 0\\ 0 \end{pmatrix}, \tag{74}$$

where $s_{ij}^{(a)}$, $s_{26}^{(a)}$ and $s_{36}^{(a)}$, $(i = 1,2,3,4; j = 1,2,3)$, are functions of the frequencies, given in Appendix B. Non-trivial solutions for C_1, C_2, C_3, and C_6 implies that the determinant of the coefficients matrix of Eq. (74) vanishes, namely,

$$\begin{vmatrix} s_{11}^{(a)} & s_{12}^{(a)} & s_{13}^{(a)} & 0\\ s_{21}^{(a)} & s_{22}^{(a)} & s_{23}^{(a)} & s_{26}^{(a)}\\ s_{31}^{(a)} & s_{32}^{(a)} & s_{33}^{(a)} & s_{36}^{(a)}\\ s_{41}^{(a)} & s_{42}^{(a)} & s_{43}^{(a)} & 0 \end{vmatrix} = 0. \tag{75}$$

Solving Eq. (75) for ω gives the frequencies of flexural free vibrations.

(b) Simply supported edge (hard type)

At the edge $r = r_0$, the transverse displacement w, the resist bending moment in the z–r plane M_{rr}, and the rotation in tangent plane ψ_θ vanish, namely,

$$\begin{aligned} &w(r_0,\theta,t) = 0,\\ &M_{rr}(r_0,\theta,t) = 0,\\ &\psi_\theta(r_0,\theta,t) = 0. \end{aligned} \tag{76}$$

Of course, Eq. (73) should also be satisfied. If the solutions for w, ψ_r, ψ_θ, and φ are substituted into Eqs. (76) and (73), four linear equations in terms of the arbitrary constants, C_1, C_2, C_3, and C_6, are obtained, namely,

$$\begin{pmatrix} s_{11}^{(b)} & s_{12}^{(b)} & s_{13}^{(b)} & 0\\ s_{21}^{(b)} & s_{22}^{(b)} & s_{23}^{(b)} & s_{26}^{(b)}\\ s_{31}^{(b)} & s_{32}^{(b)} & s_{33}^{(b)} & s_{36}^{(b)}\\ s_{41}^{(b)} & s_{42}^{(b)} & s_{43}^{(b)} & s_{46}^{(b)} \end{pmatrix} \begin{pmatrix} C_1\\ C_2\\ C_3\\ C_6 \end{pmatrix} = \begin{pmatrix} 0\\ 0\\ 0\\ 0 \end{pmatrix}, \tag{77}$$

where the coefficients, $s_{ij}^{(b)}$, $s_{26}^{(b)}$, $s_{36}^{(b)}$ and $s_{46}^{(b)}$, $(i = 1,2,3,4; j = 1,2,3)$, are given in Appendix B. To obtain non-trivial solutions for C_1, C_2, C_3, and C_6, the determinant of the coefficients matrix of Eq. (77) must vanish, from which the frequencies, ω, can be obtained.

(c) Simply supported edge (soft type)

At the edge $r = r_0$, the transverse displacement w, the resist bending moment in the z–r plane and the z–θ plane, M_{rr} and $M_{r\theta}$ (instead of ψ_θ), vanish, namely,

$$\begin{aligned} &w(r_0, \theta, t) = 0, \\ &M_{rr}(r_0, \theta, t) = 0, \\ &M_{r\theta}(r_0, \theta, t) = 0. \end{aligned} \tag{78}$$

Obviously Eq. (73) should be satisfied again. If the solutions for w, ψ_r, ψ_θ, and φ are substituted into Eqs. (78) and (73), Eq. (77) is obtained again, but the coefficients, $s_{3n}^{(b)}$, $s_{36}^{(b)}$, $n = 1, 2, 3$, are replaced by $s_{3n}^{(c)}$ and $s_{36}^{(c)}$ which are defined in Appendix B. The frequencies, ω, can be obtained again from the condition that the determinant of the coefficients matrix must vanish.

4.5. Mode shapes

It is noted that only three of the four equations in Eqs. (74) or (77) are linearly independent. Thus, C_1, C_2, and C_6 can be expressed in terms of C_3 by solving the first equations of Eqs. (74) or (77), as follows:

$$\begin{aligned} C_1 &= C_{C1} C_3, \\ C_2 &= C_{C2} C_3, \\ C_6 &= C_{C6} C_3, \end{aligned} \tag{79}$$

where the coefficients, C_{C1}, C_{C2}, and C_{C6}, are given in Appendix B.

Substituting Eq. (79) into the solutions for w, ψ_r, ψ_θ, and φ, which we obtained in the proceeding sections, yield the mode shapes of w, ψ_r, ψ_θ, and φ, respectively.

The normal modes of the transverse displacement $\bar{w}(r, \theta)$ are given by

$$\bar{w}(r, \theta) = \sum_{n=1}^{3} C_{Cn} Z_{np}(\alpha_n r) \begin{pmatrix} \sin(p\theta) \\ \cos(p\theta) \end{pmatrix}, \tag{80}$$

where to get a close form we let $C_{C3} = 1$; C_{C1} and C_{C2} are given in Appendix B.

The normal modes of the rotation in the z–r plane $\bar{\psi}_r(r, \theta)$ are given by

$$\begin{aligned} &\psi_r(r, \theta, t) \\ &\quad = \left\{ \frac{G_2/A_{10}}{A_{10}A_3A_6G_1 - A_3A_5 + A_3A_6 - A_4A_6\omega^2} \sum_{n=1}^{3} \left[\frac{G_1(A_9A_3 - A_6A_8)x_n^2 + (G_1A_7A_9\omega^2 - G_1A_3A_{10} - A_3)x_n}{A_3 - A_4\omega^2} \right.\right. \\ &\qquad + \frac{A_5(A_9A_3 - A_6A_8)x_n + A_5A_9A_7\omega^2 - A_6A_{10}A_3}{G_2} \\ &\qquad \left.\left. - \frac{A_3A_5(A_8 - 1)x_n + A_{10}A_3^2 + (A_{10}D_1 + A_{10}D_2 - A_5)A_7\omega^2}{(A_6 - A_3A_9)(A_3 - A_4\omega^2)} \right] C_{Cn}\alpha_n Z'_{np}(\alpha_n r) + \frac{C_{C6}pZ_{6p}(\beta_1 r)}{r} \right\} \\ &\qquad \times \begin{pmatrix} \sin(p\theta) \\ \cos(p\theta) \end{pmatrix}. \end{aligned} \tag{81}$$

The normal modes of the rotation in the tangent plane $\overline{\psi}_\theta(r,\theta)$ are given by

$$\begin{aligned}\psi_\theta(r,\theta,t) &= \left\{ \frac{pG_2/A_{10}}{A_{10}A_3A_6G_1 - A_3A_5 + A_3A_6 - A_4A_6\omega^2} \sum_{n=1}^{3} \left[\frac{G_1(A_9A_3 - A_6A_8)x_n^2 + (G_1A_7A_9\omega^2 - G_1A_3A_{10} - A_3)x_n}{A_3 - A_4\omega^2} \right.\right. \\ &\quad + \frac{A_5(A_9A_3 - A_6A_8)x_n + A_5A_9A_7\omega^2 - A_6A_{10}A_3}{G_2} \\ &\quad \left.\left. - \frac{A_3A_5(A_8-1)x_n + A_{10}A_3^2 + (A_{10}D_1 + A_{10}D_2 - A_5)A_7\omega^2}{(A_6 - A_3A_9)(A_3 - A_4\omega^2)} \right] \frac{C_{Cn}Z_{np}(\alpha_n r)}{r} + C_{C6}\beta_1 Z'_{6p}(\beta_1 r) \right\} \\ &\quad \times \begin{pmatrix} \cos(p\theta) \\ -\sin(p\theta) \end{pmatrix}. \end{aligned} \tag{82}$$

The normal modes of the electric potential $\bar{\varphi}(r,\theta)$ are given by

$$\begin{aligned}\varphi(r,\theta,t) = \sum_{n=1}^{3} \left\{ \frac{G_2(A_3 - A_4\omega^2 - D_1x_n - D_2x_n)}{A_5A_{10}(A_{10}A_3A_6G_1 - A_3A_5 + A_3A_6 - A_4A_6\omega^2)} \right. \\ \times \left[\frac{G_1(A_9A_3 - A_6A_8)x_n^2 + (G_1A_7A_9\omega^2 - G_1A_3A_{10} - A_3)x_n}{A_3 - A_4\omega^2} \right. \\ + \frac{A_5(A_9A_3 - A_6A_8)x_n + A_5A_9A_7\omega^2 - A_6A_{10}A_3}{G_2} \\ \left.\left. - \frac{A_3A_5(A_8-1)x_n + A_{10}A_3^2 + (A_{10}D_1 + A_{10}D_2 - A_5)A_7\omega^2}{(A_6 - A_3A_9)(A_3 - A_4\omega^2)} \right] + \frac{A_3}{A_5} \right\} C_{Cn}Z_{np}(\alpha_n r) \\ \times \begin{pmatrix} \sin(p\theta) \\ \cos(p\theta) \end{pmatrix}. \end{aligned} \tag{83}$$

5. Numerical examples and discussion

The numerical solution for a three-layer laminated plate shown in Fig. 1 is investigated. The host material is used by steel and the piezoelectric layer is PZT4. The piezoelectric layers are poled in the thickness direction and both surfaces of each layer are short-circuited. The material properties are listed in Table 1. The thickness of the host layer and piezoelectric layers are 20 and 2 mm, respectively. Four plates of different radii, 0.6, 0.3, 0.2, and 0.1 m, are studied. The results are compared with those of 3D FEA and the analytical model (Wang et al., 2001) based on Kirchhoff's CPT. Two kinds of boundary conditions, clamped edges and simply supported edges, are investigated. To investigate the effect of piezoelectric layer, four single-layer plates, the dimension and properties of which are identical to those of the host material of the three-layer piezoelectric coupled plates, are also analysed, and the results compared. The 3D FEAs were carried out using ABAQUS 6.1.

5.1. Clamped edges

Tables 2–5 list comparisons of the frequencies calculated for clamped edges by the IPT-based model (proposed), the CPT-based model (Wang et al., 2001), and 3D FEA, where Table 2 is for $r_0 = 0.6m$, Table 3 for $r_0 = 0.3m$, Table 4 for $r_0 = 0.2m$, and Table 5 for $r_0 = 0.1m$. The following notations are adopted in the tables: ω_{p_fem} represents the flexural vibration frequency of the piezoelectric laminate plate obtained by

Table 1
Material properties of the piezoelectric coupled plate

Property	Structural layer	Piezoelectric layer
E (GPa)	200	–
μ	0.3	–
C_{11}^E (GPa)	–	132
C_{12}^E (GPa)	–	71
C_{33}^E (GPa)	–	115
C_{13}^E (GPa)	–	73
C_{55}^E (GPa)	–	26
e_{31} ($\mathrm{C\,m^{-2}}$)	–	−4.1
e_{33} ($\mathrm{C\,m^{-2}}$)	–	14.1
e_{15} ($\mathrm{C\,m^{-2}}$)	–	10.5
Ξ_{11} ($\mathrm{nF\,m^{-1}}$)	–	7.124
Ξ_{33} ($\mathrm{nF\,m^{-1}}$)	–	5.841
ρ ($\mathrm{kg\,m^{-3}}$)	7800	7500

Table 2
Comparison of frequencies for $r_0/h = 60$ (clamped edge)

p	m	ω_{p_fem} (rad/s)	ω_{p_min} (rad/s)	ω_{p_kir} (rad/s)	$\omega_{p\_\mathrm{min}}/\omega_{p\_\mathrm{fem}}$	$\omega_{p\_\mathrm{kir}}/\omega_{p\_\mathrm{fem}}$
0	1	900.1	899.1	902.5	0.999	1.003
1	1	1862.7	1864.1	1878.2	1.001	1.008
2	1	3050.9	3044.7	3081.1	0.998	1.010
0	2	3475.2	3468.3	3513.4	0.998	1.011
1	2	5272.1	5272.6	5373.7	1.000	1.019
2	2	7306.2	7283.0	7472.1	0.997	1.023

Table 3
Comparison of frequencies for $r_0/h = 30$ (clamped edge)

p	m	ω_{p_fem} (rad/s)	ω_{p_min} (rad/s)	ω_{p_kir} (rad/s)	$\omega_{p\_\mathrm{min}}/\omega_{p\_\mathrm{fem}}$	$\omega_{p\_\mathrm{kir}}/\omega_{p\_\mathrm{fem}}$
0	1	3567.7	3556.0	3609.9	0.997	1.012
1	1	7295.5	7295.2	7512.7	1.000	1.030
2	1	11844.0	11775.6	12324.3	0.994	1.041
0	2	13456.0	13375.0	14053.7	0.994	1.044
1	2	20075.0	20017.1	21494.7	0.997	1.071
2	2	27467.0	27205.5	29888.5	0.990	1.088

Table 4
Comparison of frequencies for $r_0/h = 20$ (clamped edge)

p	m	ω_{p_fem} (rad/s)	ω_{p_min} (rad/s)	ω_{p_kir} (rad/s)	$\omega_{p\_\mathrm{min}}/\omega_{p\_\mathrm{fem}}$	$\omega_{p\_\mathrm{kir}}/\omega_{p\_\mathrm{fem}}$
0	1	7901.5	7857.2	8122.3	0.994	1.028
1	1	15890.0	15864.1	16903.5	0.998	1.064
2	1	25449.0	25186.8	27729.7	0.990	1.090
0	2	28802.0	28491.8	31620.9	0.989	1.098
1	2	42095.0	41794.6	48363.1	0.993	1.149
2	2	56658.0	55735.4	67249.2	0.984	1.187

FEA; ω_{p_min} the frequency calculated using the IPT-based model; ω_{p_kir} the frequency using the CPT-based model; ω_{e_fem} the flexural frequency of the one-layer plate obtained by 3D FEA; p is the wave number in the circumferential direction; m is the index of the flexural modes for a certain wave number.

Table 5
Comparison of frequencies for $r_0/h = 10$ (clamped edge)

p	m	ω_{p_fem} (rad/s)	ω_{p_min} (rad/s)	ω_{p_kir} (rad/s)	$\omega_{p\_min}/\omega_{p\_fem}$	$\omega_{p\_kir}/\omega_{p\_fem}$
0	1	29229.0	28816.8	32489.2	0.986	1.112
1	1	55213.0	54678.6	67614.1	0.990	1.225
2	1	84292.0	82297.6	110918.9	0.976	1.316
0	2	94232.0	91902.8	126483.5	0.975	1.342
1	2	130382.0	127771.0	193452.4	0.980	1.484
2	2	168570.0	163167.0	268996.8	0.968	1.596

As shown in Table 2, for a thin plate with a very large diameter–thickness ratio, such as $r_0/h = 60$, the frequencies from both CPT-based model and IPT-based model are in close agreement with the FEA results. The IPT-based model produces results almost coincident with those of FEA while the results from CPT-based model differs less than 2.3%. Tables 3–5 show that, as the diameter–thickness ratio increases, the proposed IPT-based model provides results similar to those of FEA with a maximum difference of only 3.2%. However, the frequencies computed by the CPT-based model can be as large as 60% greater than those by FEA (for the case of a thick plate with a diameter–thickness ratio of 10). Both the CPT-based and IPT-based models give results closer to the FEA results at lower frequencies than they do at higher frequencies. As shown in Table 5, the CPT-based model gives a frequency 59.6% greater than that of the FEA in case of $p = 2$ and $m = 2$ while it gives a value only 11.2% greater for the first mode. The CPT-based model gives greater frequencies than the IPT-based model because the CPT neglects the effect of transverse shear deformation and rotatory inertia and hence overestimates the frequencies. Fig. 3 shows frequency ratios of the three-layered plates to those of one-layered plates for the following cases: $r_0/h = 60$, 30, 20, and 10. It seems that the piezoeffects are more obvious on plates with a higher diameter–thickness ratio than on that with a lower one when piezoelectric layers of same thickness are attached.

5.2. Simply supported edges

Tables 6–9 compare the frequencies calculated for circular plates with simply supported edge by the IPT-based model, the CPT-based model, and 3D FEA, where Table 6 is for $r_0 = 0.6m$, Table 7 for $r_0 = 0.3m$,

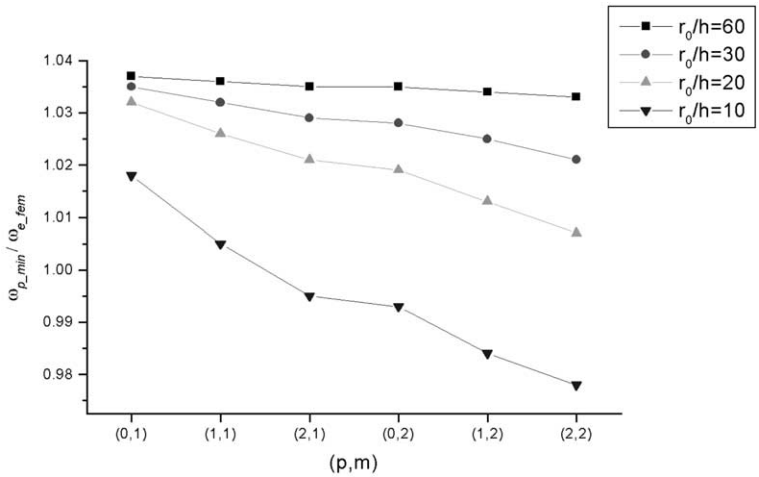

Fig. 3. Effect of thickness of piezoelectric layers on frequencies to plates (clamped edge).

Table 6
Comparison of frequencies for $r_0/h = 60$ (simply supported edge)

p	m	ω_{p_fem} (rad/s)	ω_{p_min} (rad/s)	ω_{p_kir} (rad/s)	$\omega_{p\_\text{min}}/\omega_{p\_\text{fem}}$	$\omega_{p\_\text{kir}}/\omega_{p\_\text{fem}}$
0	1	435.2	435.1	435.6	1.000	1.001
1	1	1218.5	1221.4	1227.5	1.002	1.007
2	1	2242.4	2241.1	2262.4	0.999	1.009
0	2	2606.5	2605.5	2625.2	1.000	1.007
1	2	4221.0	4228.7	4282.4	1.002	1.015
2	2	6088.3	6079.5	6193.9	0.999	1.017

Table 7
Comparison of frequencies for $r_0/h = 30$ (simply supported edge)

p	m	ω_{p_fem} (rad/s)	ω_{p_min} (rad/s)	ω_{p_kir} (rad/s)	$\omega_{p\_\text{min}}/\omega_{p\_\text{fem}}$	$\omega_{p\_\text{kir}}/\omega_{p\_\text{fem}}$
0	1	1735.3	1734.4	1742.5	1.000	1.004
1	1	4810.2	4828.6	4910.0	1.004	1.021
2	1	8792.1	8771.6	9049.7	0.998	1.029
0	2	10222.0	10197.9	10500.9	0.998	1.027
1	2	16316.0	16334.6	17129.7	1.001	1.050
2	2	23278.0	23148.1	24775.9	0.994	1.064

Table 8
Comparison of frequencies for $r_0/h = 20$ (simply supported edge)

p	m	ω_{p_fem} (rad/s)	ω_{p_min} (rad/s)	ω_{p_kir} (rad/s)	$\omega_{p\_\text{min}}/\omega_{p\_\text{fem}}$	$\omega_{p\_\text{kir}}/\omega_{p\_\text{fem}}$
0	1	3884.0	3879.5	3920.7	0.999	1.010
1	1	10623.0	10671.1	11047.4	1.005	1.040
2	1	19209.0	19114.5	20361.9	0.995	1.060
0	2	22301.0	22186.4	23627.1	0.995	1.060
1	2	34940.0	34903.9	38541.9	0.999	1.103
2	2	49098.0	48572.9	55745.7	0.989	1.135

Table 9
Comparison of frequencies for $r_0/h = 10$ (simply supported edge)

p	m	ω_{p_fem} (rad/s)	ω_{p_min} (rad/s)	ω_{p_kir} (rad/s)	$\omega_{p\_\text{min}}/\omega_{p\_\text{fem}}$	$\omega_{p\_\text{kir}}/\omega_{p\_\text{fem}}$
0	1	15122.0	15059.1	15682.9	0.996	1.037
1	1	39205.0	39321.9	44189.7	1.003	1.127
2	1	67828.0	66843.9	81447.7	0.986	1.201
0	2	78080.0	76888.6	94508.6	0.985	1.210
1	2	115525.0	114276.4	154167.4	0.989	1.334
2	2	155227.0	151364.6	222982.9	0.975	1.436

Table 8 for $r_0 = 0.2m$, and Table 9 for $r_0 = 0.1m$. Fig. 4 plots frequency ratios of the three-layered plates to those of one-layered plates for the four cases: $r_0/h = 60$, 30, 20, and 10. The findings for the clamped plates are reflected again by the simply supported cases.

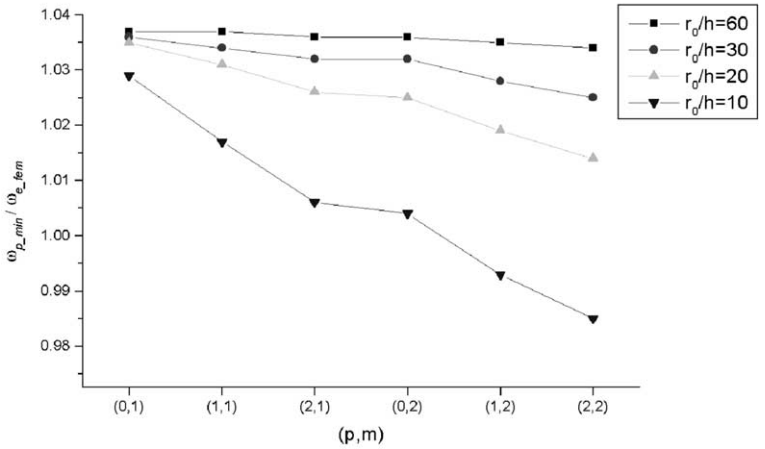

Fig. 4. Effect of thickness of piezoelectric layers on frequencies to plates (simply supported edge).

6. Conclusions

An analytical solution of free flexural vibration of a three-layered piezoelectric laminated circular moderately thick plate is proposed based on the Mindlin's plate theory for the cases where the electrodes on the piezoelectric layers are shortly connected. The electric potential distribution across thickness of piezoelectric layers is modelled by a sinusoidal function. Hence the Maxwell equation is enforced. The mathematical derivation was presented in detail. Numerical investigations were performed for plates with various diameter–thickness ratios and with two kinds of boundary conditions, clamped edge and simply supported edge. The validity of the solution based on IPT model for diameter–thickness ratios not less than 10 was verified by the 3D FEAs. The CPT-based model proved to be valid only for thin plates and diverge from the FEA results for thick plates, particularly for high frequencies.

Acknowledgements

The work in this paper is supported by the research grant from National University of Singapore, R-264-000-057-112.

Appendix A

The piezoelectric material is transversely isotropic material where for planes normal to the poling direction, the material properties are equivalent in all directions. For plate problems, the 2D or 1D constitutive relationships can be reduced from the 3D constitutive relationship. Without losing arbitrariness, a coordinate system is adopted where the thickness direction of plate is in axis 3, as shown in Fig. 5. If the piezoelectric material is poled in direction 3, its constitutive relationship is given by (Tiersten, 1969)

$$\begin{Bmatrix}\sigma_{11}\\ \sigma_{22}\\ \sigma_{33}\\ \sigma_{12}\\ \sigma_{13}\\ \sigma_{23}\end{Bmatrix} = \begin{pmatrix} C_{11}^E & C_{12}^E & C_{13}^E & 0 & 0 & 0\\ C_{12}^E & C_{11}^E & C_{13}^E & 0 & 0 & 0\\ C_{13}^E & C_{13}^E & C_{33}^E & 0 & 0 & 0\\ 0 & 0 & 0 & \frac{1}{2}(C_{11}^E - C_{12}^E) & 0 & 0\\ 0 & 0 & 0 & 0 & C_{55}^E & 0\\ 0 & 0 & 0 & 0 & 0 & C_{55}^E \end{pmatrix} \begin{Bmatrix}\varepsilon_{11}\\ \varepsilon_{22}\\ \varepsilon_{33}\\ \gamma_{12}\\ \gamma_{13}\\ \gamma_{23}\end{Bmatrix} - \begin{pmatrix} 0 & 0 & e_{31}\\ 0 & 0 & e_{31}\\ 0 & 0 & e_{33}\\ 0 & 0 & 0\\ e_{15} & 0 & 0\\ 0 & e_{15} & 0 \end{pmatrix} \begin{Bmatrix}E_1\\ E_2\\ E_3\end{Bmatrix}, \qquad (A.1)$$

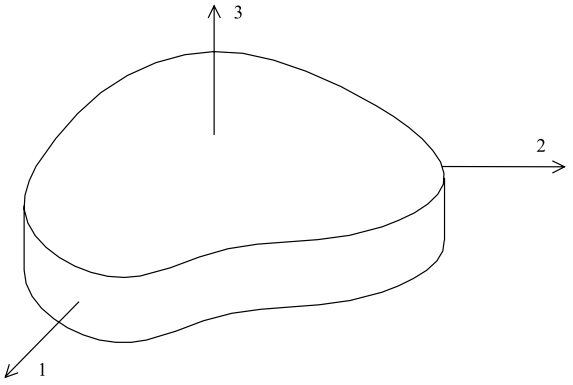

Fig. 5. Coordinate system for plates.

$$\begin{Bmatrix} D_1 \\ D_2 \\ D_3 \end{Bmatrix} = \begin{pmatrix} 0 & 0 & 0 & 0 & e_{15} & 0 \\ 0 & 0 & 0 & 0 & 0 & e_{15} \\ e_{31} & e_{31} & e_{33} & 0 & 0 & 0 \end{pmatrix} \begin{Bmatrix} \varepsilon_{11} \\ \varepsilon_{22} \\ \varepsilon_{33} \\ \gamma_{12} \\ \gamma_{13} \\ \gamma_{23} \end{Bmatrix} + \begin{pmatrix} \Xi_{11} & 0 & 0 \\ 0 & \Xi_{11} & 0 \\ 0 & 0 & \Xi_{33} \end{pmatrix} \begin{Bmatrix} E_1 \\ E_2 \\ E_3 \end{Bmatrix}, \tag{A.2}$$

where σ_{11}, σ_{22}, σ_{33}, σ_{12}, σ_{13}, and σ_{23} are the stress components; ε_{11}, ε_{22}, ε_{33}, γ_{12}, γ_{13}, and γ_{23} the engineering strain components; D_1, D_2, and D_3 the electric displacements; E_1, E_2, and E_3 the electric field intensities; C_{11}^E, C_{33}^E, C_{12}^E, C_{13}^E, and C_{55}^E the elasticity moduli at constant electric field; e_{31}, e_{33}, and e_{15} the piezoelectric strain coefficients; and Ξ_{11}, and Ξ_{33} the dielectric constants.

Solving $\sigma_{33} = 0$ for $\varepsilon_{33} = 0$ gives

$$\varepsilon_{33} = \frac{e_{33}}{C_{33}^E} E_3 - \frac{C_{13}^E}{C_{33}^E}(\varepsilon_{11} + \varepsilon_{22}). \tag{A.3}$$

Substituting Eq. (A.3) into Eqs. (A.1) and (A.2) yields

$$\begin{Bmatrix} \sigma_{11} \\ \sigma_{22} \\ \sigma_{12} \\ \sigma_{13} \\ \sigma_{23} \end{Bmatrix} = \begin{pmatrix} \overline{C}_{11}^E & \overline{C}_{12}^E & 0 & 0 & 0 \\ \overline{C}_{12}^E & \overline{C}_{11}^E & 0 & 0 & 0 \\ 0 & 0 & \frac{1}{2}(\overline{C}_{11}^E - \overline{C}_{12}^E) & 0 & 0 \\ 0 & 0 & 0 & C_{55}^E & 0 \\ 0 & 0 & 0 & 0 & C_{55}^E \end{pmatrix} \begin{Bmatrix} \varepsilon_{11} \\ \varepsilon_{22} \\ \gamma_{12} \\ \gamma_{13} \\ \gamma_{23} \end{Bmatrix} - \begin{pmatrix} 0 & 0 & \bar{e}_{31} \\ 0 & 0 & \bar{e}_{31} \\ 0 & 0 & 0 \\ e_{15} & 0 & 0 \\ 0 & e_{15} & 0 \end{pmatrix} \begin{Bmatrix} E_1 \\ E_2 \\ E_3 \end{Bmatrix}, \tag{A.4}$$

$$\begin{Bmatrix} D_1 \\ D_2 \\ D_3 \end{Bmatrix} = \begin{pmatrix} 0 & 0 & 0 & e_{15} & 0 \\ 0 & 0 & 0 & 0 & e_{15} \\ \bar{e}_{31} & \bar{e}_{31} & 0 & 0 & 0 \end{pmatrix} \begin{Bmatrix} \varepsilon_{11} \\ \varepsilon_{22} \\ \gamma_{12} \\ \gamma_{13} \\ \gamma_{23} \end{Bmatrix} + \begin{pmatrix} \Xi_{11} & 0 & 0 \\ 0 & \Xi_{11} & 0 \\ 0 & 0 & \overline{\Xi}_{33} \end{pmatrix} \begin{Bmatrix} E_1 \\ E_2 \\ E_3 \end{Bmatrix}. \tag{A.5}$$

where $\overline{C}_{11}^E$, $\overline{C}_{12}^E$, $\bar{e}_{31}$, and $\overline{\Xi}_{33}$ are given by

$$\begin{aligned} &\overline{C}_{11}^E = C_{11}^E - \frac{(C_{13}^E)^2}{C_{33}^E}, \quad \overline{C}_{12}^E = C_{12}^E - \frac{(C_{13}^E)^2}{C_{33}^E}, \\ &\bar{e}_{31} = e_{31} - \frac{C_{13}^E}{C_{33}^E} e_{33}, \quad \overline{\Xi}_{33} = \Xi_{33} + \frac{e_{33}^2}{C_{33}^E}. \end{aligned} \tag{A.6}$$

If the transverse shear stiffness is modified by a shear factor κ^2, Eq. (A.4) becomes

$$\begin{Bmatrix}\sigma_{11}\\ \sigma_{22}\\ \sigma_{12}\\ \sigma_{13}\\ \sigma_{23}\end{Bmatrix}=\begin{pmatrix}\overline{C}_{11}^{E} & \overline{C}_{12}^{E} & 0 & 0 & 0\\ \overline{C}_{12}^{E} & \overline{C}_{11}^{E} & 0 & 0 & 0\\ 0 & 0 & \frac{1}{2}(\overline{C}_{11}^{E}-\overline{C}_{12}^{E}) & 0 & 0\\ 0 & 0 & 0 & \kappa^2 C_{55}^{E} & 0\\ 0 & 0 & 0 & 0 & \kappa^2 C_{55}^{E}\end{pmatrix}\begin{Bmatrix}\varepsilon_{11}\\ \varepsilon_{22}\\ \gamma_{12}\\ \gamma_{13}\\ \gamma_{23}\end{Bmatrix}-\begin{pmatrix}0 & 0 & \bar{e}_{31}\\ 0 & 0 & \bar{e}_{31}\\ 0 & 0 & 0\\ e_{15} & 0 & 0\\ 0 & e_{15} & 0\end{pmatrix}\begin{Bmatrix}E_1\\ E_2\\ E_3\end{Bmatrix}. \tag{A.7}$$

Appendix B

Some coefficients referred to in this paper are given as follows:

$$\begin{aligned}
&A_1=\frac{1}{2}\left[(1-\mu)D_1+\left(1-\frac{\overline{C}_{12}^{E}}{\overline{C}_{11}^{E}}\right)D_2\right],\quad A_2=\frac{1}{2}\left[(1+\mu)D_1+\left(1+\frac{\overline{C}_{12}^{E}}{\overline{C}_{11}^{E}}\right)D_2\right],\\
&A_3=\kappa^2\frac{Eh}{1+\mu}+2\kappa^2 C_{55}^{E}h_1,\quad A_4=\tfrac{2}{3}\left[h^3\rho_1+h_1(3h^2+3hh_1+h_1^2)\rho_2\right],\quad A_5=\frac{4h_1(e_{15}-\bar{e}_{31})}{\pi},\\
&A_6=\frac{4h_1e_{15}}{\pi},\quad A_7=2h\rho_1+2h_1\rho_2,\quad A_8=\frac{e_{15}}{e_{15}+\bar{e}_{31}},\quad A_9=\frac{2\overline{\Xi}_{11}}{\pi(e_{15}+\bar{e}_{31})},\quad A_{10}=\frac{2\pi\overline{\Xi}_{33}}{h_1^2(e_{15}+\bar{e}_{31})};
\end{aligned} \tag{B.1}$$

$$\begin{aligned}
P_1&=(D_1+D_2)(2h_1e_{15}^2-\overline{\Xi}_{11}A_3),\\
P_2&=A_3\left[2h_1\bar{e}_{31}^2+\frac{\pi^2\overline{\Xi}_{33}(D_1+D_2)}{h_1^2}\right],\\
P_3&=A_4(A_3\overline{\Xi}_{11}-2h_1e_{15}^2)+A_7\overline{\Xi}_{11}(D_1+D_2),\\
P_4&=-A_7A_4\overline{\Xi}_{11},\\
P_5&=2A_7h_1(e_{15}^2-\bar{e}_{31}^2)-\frac{[A_7(D_1+D_2)+A_4A_3]\pi^2\overline{\Xi}_{33}}{h_1^2}-A_7A_3\overline{\Xi}_{11},\\
P_6&=\frac{\pi^2A_7A_3\overline{\Xi}_{33}}{h_1^2},\\
P_7&=\frac{\pi^2A_7A_4\overline{\Xi}_{33}}{h_1^2}.
\end{aligned} \tag{B.2}$$

$$G_1=\frac{(D_1+D_2)}{(\mathrm{A}_6-A_3A_9)},\quad G_2=A_5(A_9A_3-A_6)+A_6A_{10}(D_1+D_2); \tag{B.3}$$

$$s_{1n}^{(a)}=Z_{np}(\alpha_nr_0),\quad s_{26}^{(a)}=pZ_{6p}(\beta_1r_0)/r_0,\quad s_{36}^{(a)}=\beta_1Z'_{6p}(\beta_1r_0), \tag{B.4}$$

$$\begin{aligned}
s_{2n}^{(a)}=\frac{G_2/A_{10}}{A_{10}A_3A_6G_1-A_3A_5+A_3A_6-A_4A_6\omega^2}\Bigg[&\frac{G_1(A_9A_3-A_6A_8)x_n^2+(G_1A_7A_9\omega^2-G_1A_3A_{10}-A_3)x_n}{A_3-A_4\omega^2}\\
&+\frac{A_5(A_9A_3-A_6A_8)x_n+A_5A_9A_7\omega^2-A_6A_{10}A_3}{G_2}\\
&-\frac{A_3A_5(A_8-1)x_n+A_{10}A_3^2+(A_{10}D_1+A_{10}D_2-A_5)A_7\omega^2}{(A_6-A_3A_9)(A_3-A_4\omega^2)}\Bigg]\alpha_nZ'_{np}(\alpha_nr_0),
\end{aligned}$$

$$s_{3n}^{(a)} = \frac{pG_2/A_{10}}{A_{10}A_3A_6G_1 - A_3A_5 + A_3A_6 - A_4A_6\omega^2}\left[\frac{G_1(A_9A_3 - A_6A_8)x_n^2 + (G_1A_7A_9\omega^2 - G_1A_3A_{10} - A_3)x_n}{A_3 - A_4\omega^2}\right.$$

$$+\frac{A_5(A_9A_3 - A_6A_8)x_n + A_5A_9A_7\omega^2 - A_6A_{10}A_3}{G_2}$$

$$\left.-\frac{A_3A_5(A_8 - 1)x_n + A_{10}A_3^2 + (A_{10}D_1 + A_{10}D_2 - A_5)A_7\omega^2}{(A_6 - A_3A_9)(A_3 - A_4\omega^2)}\right]\frac{Z_{np}(\alpha_n r_0)}{r_0},$$

$$s_{4n}^{(a)} = \left\{\frac{2\overline{\Xi}_{11}G_2(D_1x_n + D_2x_n - A_3 + A_4\omega^2)}{\pi e_{15}A_5A_{10}(A_{10}A_3A_6G_1 - A_3A_5 + A_3A_6 - A_4A_6\omega^2)}\left[\frac{G_1(A_9A_3 - A_6A_8)x_n^2 + (G_1A_7A_9\omega^2 - G_1A_3A_{10} - A_3)x_n}{A_3 - A_4\omega^2}\right.\right.$$

$$\left.+\frac{A_5(A_9A_3 - A_6A_8)x_n + A_5A_9A_7\omega^2 - A_6A_{10}A_3}{G_2} - \frac{A_3A_5(A_8 - 1)x_n + A_{10}A_3^2 + (A_{10}D_1 + A_{10}D_2 - A_5)A_7\omega^2}{(A_6 - A_3A_9)(A_3 - A_4\omega^2)}\right]$$

$$\left.-\frac{2\overline{\Xi}_{11}A_3}{\pi e_{15}A_5} + 1\right\}\alpha_n Z'_{np}(\alpha_n r_0), \quad (n = 1, 2, 3);$$

$$s_{1n}^{(b)} = Z_{np}(\alpha_n r_0),$$

$$s_{26}^{(b)} = 2p\left(\frac{\beta_1 Z'_{6p}(\beta_1 r_0)}{r_0} - \frac{Z_{6p}(\beta_1 r_0)}{r_0^2}\right), \quad s_{36}^{(b)} = \beta_1 Z'_{6p}(\beta_1 r_0), \tag{B.5}$$

$$s_{2n}^{(b)} = \frac{G_2/A_{10}}{A_{10}A_3A_6G_1 - A_3A_5 + A_3A_6 - A_4A_6\omega^2}\left[\frac{G_1(A_9A_3 - A_6A_8)x_n^2 + (G_1A_7A_9\omega^2 - G_1A_3A_{10} - A_3)x_n}{A_3 - A_4\omega^2}\right.$$

$$+\frac{A_5(A_9A_3 - A_6A_8)x_n + A_5A_9A_7\omega^2 - A_6A_{10}A_3}{G_2}$$

$$\left.-\frac{A_3A_5(A_8 - 1)x_n + A_{10}A_3^2 + (A_{10}D_1 + A_{10}D_2 - A_5)A_7\omega^2}{(A_6 - A_3A_9)(A_3 - A_4\omega^2)}\right]$$

$$\times\left[\frac{2A_1p^2}{r_0^2}Z_{np}(\alpha_n r_0) + \frac{e_{15}(A_1 + A_2)x_n - \bar{e}_{31}(A_3 - A_4\omega^2)}{e_{15} - \bar{e}_{31}}Z_{np}(\alpha_n r_0) - \frac{2A_1\alpha_n}{r_0}Z'_{np}(\alpha_n r_0)\right]$$

$$-\frac{A_3\bar{e}_{31}}{e_{15} - \bar{e}_{31}}Z_{np}(\alpha_n r_0),$$

$$s_{3n}^{(b)} = \frac{pG_2/A_{10}}{A_{10}A_3A_6G_1 - A_3A_5 + A_3A_6 - A_4A_6\omega^2}\left[\frac{G_1(A_9A_3 - A_6A_8)x_n^2 + (G_1A_7A_9\omega^2 - G_1A_3A_{10} - A_3)x_n}{A_3 - A_4\omega^2}\right.$$

$$+\frac{A_5(A_9A_3 - A_6A_8)x_n + A_5A_9A_7\omega^2 - A_6A_{10}A_3}{G_2}$$

$$\left.-\frac{A_3A_5(A_8 - 1)x_n + A_{10}A_3^2 + (A_{10}D_1 + A_{10}D_2 - A_5)A_7\omega^2}{(A_6 - A_3A_9)(A_3 - A_4\omega^2)}\right]\frac{Z_{np}(\alpha_n r_0)}{r_0},$$

$$s_{4n}^{(b)} = \left\{ \frac{2\overline{\Xi}_{11}G_2/A_{10}}{A_{10}A_3A_6G_1 - A_3A_5 + A_3A_6 - A_4A_6\omega^2} \left(\frac{D_1x_n + D_2x_n - A_3 + A_4\omega^2}{\pi e_{15}A_5} + \frac{1}{2\overline{\Xi}_{11}} \right) \right.$$
$$\times \left[\frac{G_1(A_9A_3 - A_6A_8)x_n^2 + (G_1A_7A_9\omega^2 - G_1A_3A_{10} - A_3)x_n}{A_3 - A_4\omega^2} \right.$$
$$+ \frac{A_5(A_9A_3 - A_6A_8)x_n + A_5A_9A_7\omega^2 - A_6A_{10}A_3}{G_2}$$
$$\left. \left. - \frac{A_3A_5(A_8 - 1)x_n + A_{10}A_3^2 + (A_{10}D_1 + A_{10}D_2 - A_5)A_7\omega^2}{(A_6 - A_3A_9)(A_3 - A_4\omega^2)} \right] - \frac{2\overline{\Xi}_{11}A_3}{\pi e_{15}A_5} + 1 \right\} \alpha_n Z'_{np}(\alpha_n r_0),$$

$$s_{46}^{(b)} = pZ_{6p}(\beta_1 r_0)/r_0, \quad (n = 1, 2, 3);$$

$$s_{3n}^{(c)} = \frac{2pG_2/A_{10}}{A_{10}A_3A_6G_1 - A_3A_5 + A_3A_6 - A_4A_6\omega^2} \left[\frac{G_1(A_9A_3 - A_6A_8)x_n^2 + (G_1A_7A_9\omega^2 - G_1A_3A_{10} - A_3)x_n}{A_3 - A_4\omega^2} \right.$$
$$+ \frac{A_5(A_9A_3 - A_6A_8)x_n + A_5A_9A_7\omega^2 - A_6A_{10}A_3}{G_2}$$
$$\left. - \frac{A_3A_5(A_8 - 1)x_n + A_{10}A_3^2 + (A_{10}D_1 + A_{10}D_2 - A_5)A_7\omega^2}{(A_6 - A_3A_9)(A_3 - A_4\omega^2)} \right] \left(\frac{\alpha_n Z'_{np}(\alpha_n r_0)}{r_0} - \frac{Z_{np}(\alpha_n r_0)}{r_0^2} \right), \tag{B.6}$$

$$s_{36}^{(c)} = -F_1 Z_{6p}(\beta_1 r_0) + 2\beta_1^2 Z''_{6p}(\beta_1 r_0), \quad (n = 1, 2, 3);$$

$$C_{C1} = \frac{s_{13}s_{26}s_{32} - s_{12}s_{26}s_{33} - s_{13}s_{22}s_{36} + s_{12}s_{23}s_{36}}{s_{12}s_{26}s_{31} - s_{11}s_{26}s_{32} - s_{12}s_{21}s_{36} + s_{11}s_{22}s_{36}},$$
$$C_{C2} = \frac{s_{11}s_{26}s_{33} - s_{13}s_{26}s_{31} + s_{13}s_{21}s_{36} - s_{11}s_{23}s_{36}}{s_{12}s_{26}s_{31} - s_{11}s_{26}s_{32} - s_{12}s_{21}s_{36} + s_{11}s_{22}s_{36}}, \tag{B.7}$$
$$C_{C6} = \frac{s_{13}s_{22}s_{31} - s_{12}s_{23}s_{31} - s_{13}s_{21}s_{32} + s_{11}s_{23}s_{32} + s_{12}s_{21}s_{33} - s_{11}s_{22}s_{33}}{s_{12}s_{26}s_{31} - s_{11}s_{26}s_{32} - s_{12}s_{21}s_{36} + s_{11}s_{22}s_{36}}.$$

References

Aldraihem, O.J., Khdeir, A.A., 2000. Smart beams with extension and thickness—shear piezoelectric actuators. Smart Mater. Struct. 9, 1–9.

Almajid, A., Taya, M., Hudnut, S., 2001. Analysis of out-of-plane displacement and stress field in a piezocomposite plate with functionally graded microstructure. Int. J. Solids Struct. 38, 3377–3391.

Bailey, T., Hubbard, J.E.J., 1985. Distributed piezoelectric polymer active vibration control of a cantilever beam. J. Guid. Cont. Dyn. 8, 605–611.

Bisegna, P., Maceri, F., 1996. An exact three-dimensional solution for simply supported rectangular piezoelectric plates. ASME J. Appl. Mech. 63, 628–638.

Chandrashekhara, K., Agarwal, A.N., 1993. Active vibration control of laminated composite plates using piezoelectric devices: a finite element approach. J. Intel. Mater. Syst. Struct. 4, 496–508.

Crawley, E.F., Anderson, E., 1989. Detailed model of piezoelectric actuation of beams. Proceedings of the 30th AIAA/ASMA/SAE Conference on Structures, Structural Dynamics, and Material. Washington, DC, April 1989, pp. 2000–2010.

Crawley, E.F., de Luis, J., 1987. Use of piezoelectric actuators as elements of intelligent structures. AIAA J. 25, 1373–1385.

Fernandes, A., Pouget, J., 2001. Two-dimensional modelling of laminated piezoelectric composites: analysis and numerical results. Thin-Walled Struct. 39, 3–22.

Hagood, N.W., McFarland, A.J., 1995. Modeling of a piezoelectric rotary ultrasonic motor. IEEE Trans. Ultrason. Ferroelectr. Freq. Cont. 44, 210–224.
Heyliger, P., 1997. Exact solutions for simply supported laminated piezoelectric plates. ASME J. Appl. Mech. 64, 299–306.
Heyliger, P.R., Ramirez, G., 2000. Free vibration of laminated circular piezoelectric plates and discs. J. Sound Vib. 229 (4), 935–956.
HKS Inc., 1993. ABAQUS User's Manual (verion 5.2). Hibbitt, Karlsson and Sorenson Inc., Providence, RI.
Huang, J.H., Wu, T.L., 1996. Analysis of hybrid multilayered piezoelectric plates. Int. J. Engng. Sci. 34 (2), 171–181.
Hwang, W.S., Park, H.C., 1993. Finite element modeling of piezoelectric sensors and actuators. AIAA J. 31, 930–937.
Khdeir, A.A., Reddy, J.N., 1997. An exact solution for the bending of thin and thickness cross-ply laminated beams. Compos. Struct. 37, 195–203.
Khdeir, A.A., Reddy, J.N., 1999. Jordan canonical form solution for thermally induced deformations of cross-ply laminated composite beams. J. Thermal Stresses 22, 331–346.
Kim, J., Varadan, V.V., Varadan, V.K., Bao, X.Q., 1996. Finite element modeling of a smart cantilever plate and comparison with experiments. Smart Mater. Struct. 5, 165–170.
Lam, K.Y., Peng, X.Q., Liu, G.R., Reddy, J.N., 1997. A finite element model for piezoelectric composite laminates. Smart Mater. Struct. 6, 583–591.
Lebrun, L., Petit, L., Briot, R., Gonnard, P., 1997. Electromechanical conversion in an ultrasonic motor using a non-axisymmetric (1,1) mode. Smart Mater. Struct. 8, 47–52.
Love, A.E.H., 1944. Treatise on the Mathematical Theory of Elasticity. Dover, New York.
Mindlin, R.D., 1951a. Influence of rotary inertia and shear on flexural motions of isotropic, elastic plates. J. Appl. Mech. 18, 31–38.
Mindlin, R.D., 1951b. Thickness-shear and flexural vibrations of crystal plates. J. Appl. Phys. 22, 316–323.
Mindlin, R.D., 1952. Forced thickness-shear and flexural vibrations of piezoelectric crystal plates. J. Appl. Phys. 23, 83–88.
Mindlin, R.D., 1955. An introduce to the mathematical theory of vibrations of elastic plates. US Army Signal Corps engineering Laboratories, Fort Monmouth, NJ.
Mindlin, R.D., 1972. High frequency vibrations of piezoelectric crystal plates. Int. J. Solids Struct. 8, 895–906.
Mindlin, R.D., 1984. Frequencies of piezoelectrically forced vibrations of electroded, doubly rotated, quartz plates. Int. J. Solids Struct. 20, 141–157.
Sheikh, A.H., Topdar, P., Halder, S., 2001. An appropriate FE model for through-thickness variation of displacement and potential in thin/moderately thick smart laminates. Compos. Struct. 51, 401–409.
So, J., Leissa, A.W., 1998. Three-dimensional vibrations of thick circular and annular plates. J. Sound Vib. 209 (1), 15–41.
Speigel, M.R., 1999. Mathematical Handbook of Formulas and Tables. Schaum's Outline Series. McGraw-Hill, Singapore.
Swanson Inc., 1993. ANSYS User's Manual, version 5.2. Swanson Inc., Houston, PA.
Tiersten, H.F., 1969. Linear Piezoelectric Plate Vibrations. Plenum Press, New York.
Timoshenko, S., Young, D.H., Weaver, W., 1974. Vibration Problems in Engineering, 4th ed. Wiley, New York.
Wang, J., Yu, J., Yong, Y.K., Imai, T., 2000. A new theory for electroded piezoelectric plates and its finite element application for the forced vibrations of quartz crystal resonators. Int. J. Solids Struct. 37, 5653–5673.
Wang, Q., Quek, S.T., 2000. Flexural vibration analysis of sandwich beam coupled with piezoelectric actuator. Smart Mater. Struct. 9, 103–109.
Wang, Q., Quek, S.T., Sun, C.T., Liu, X., 2001. Analysis of piezoelectric coupled circular plate. Smart Mater. Struct. 10, 229–239.
Whitney, J.M., Pagano, N.J., 1970. Shear deformation in heterogeneous anisotropic plates. ASME J. Appl. Mech. 37, 1031–1036.
Yu, Y.Y., 1995. Some recent advances in linear and nonlinear dynamical modelling of elastic and piezoelectric plates. J. Intel. Mater. Syst. Struct. 6, 237–254.